Article

Plasma Treatment of Polystyrene Films—Effect on Wettability and Surface Interactions with Au Nanoparticles

Mohammad Islam [1,*], Zineb Matouk [2], Nadir Ouldhamadouche [3], Jean-Jacques Pireaux [4] and Amine Achour [5,*]

1   GE Aerospace, 3290 Patterson Ave SE, Grand Rapids, MI 49512, USA
2   Technology Innovation Institute, Abu Dhabi P.O. Box 9639, United Arab Emirates
3   Laboratoire de Génie Physique, Université Ibn Khaldoun, BP P 78 Zaâroura, Tiaret 14000, Algeria
4   Research Centre, Physics of Matter and Radiation (PMR), LISE Laboratory, University of Namur, 5000 Namur, Belgium
5   Pixium Vision S.A., 74 Rue du FGB Saint-Antoine, 75012 Paris, France
*   Correspondence: mohammad.islam@gmail.com (M.I.); aachour@pixium-vision.com (A.A.)

Abstract: Polystyrene (PS)/Gold (Au) is used for a wide range of applications, including composite nanofibers, catalysis, organic memory devices, and biosensing. In this work, PS films were deposited on silicon substrates via a spin coating technique followed by treatment with argon (Ar) plasma admixed with ammonia (NH_3), oxygen (O_2), or tetrafluoroethane ($C_2H_2F_4$). X-Ray photoelectron spectroscopy (XPS) analysis revealed modified surface chemistry for Ar/O_2, Ar/NH_3, or $Ar/C_2H_2F_4$ plasma treatment through the incorporation of oxygen, nitrogen, or fluorine groups, respectively. Size-controlled magnetron sputter deposition of Au nanoparticles (NP) onto these plasma-treated PS films was investigated via XPS and AFM techniques. The interaction of the Au NPs, as probed from the XPS and AFM measurements, is discussed by referring to changes in surface chemistry and morphology of the PS after plasma treatment. The results demonstrate the effect of surface chemistry on the interaction of Au NPs with polymer support having different surface functionalities. The XPS results show that significant oxygen surface incorporation resulted from oxygen-containing species in the plasma itself. The surface concentration of O increased from 0.4% for the pristine PS to 4.5 at%, 35.4 at%, and 45.6 at% for the $Ar/C_2H_4F_4$, Ar/NH_3, and Ar/O_2, respectively. The water contact angle (WCA) values were noticed to decrease from 98° for the untreated PS to 95°, 37°, and 15° for $Ar/C_2H_2F_4$, Ar/NH_3, and Ar/O_2 plasma-modified PS samples, respectively. AFM results demonstrate that surface treatment was also accompanied by surface morphology change. Small Au islands are well dispersed and cover the surface, thus forming a homogeneous, isotropic structure. The reported results are important for exploiting Au NPs use in catalysis and sensing applications.

Keywords: gold nanoparticles; XPS; AFM; plasma treatment; surface chemistry

1. Introduction

Polystyrene (PS) is a polymer material that is extensively used in industry due to its low cost, cyclability, and excellent physical–chemical properties, such as being lightweight and having chemical and mechanical stabilities [1]. PS is used for different applications, including food packaging [2], transparent solid tools [3], and thermal insulators [4]. This polymer is hydrophobic in nature; however, for some specific applications, hydrophilic PS is needed for use as a biosensing platform [5], surface protection, or smart coatings [4].

A promising technique for the modification of chemical and physical properties of polymer surfaces without impacting the bulk material is plasma treatment [6–8]. Although plasma treatment is frequently used, there is still some debate over the relative significance of the many plasma–polymer interactions that take place at the surface that can result in the production of free radical sites. Oxygen plasma treatment has been widely reported to increase the wettability and adhesion of polar polymers such as PS [9]. Nonetheless, the effect of different plasma treatments is rarely reported. Exploring different plasma

chemistries would allow us not only to tune the surface hydrophilicity but also to graft other chemical groups that could keep the surface hydrophobic yet allow their use for different purposes.

A variety of techniques, including wet chemistry, electro-plating, sonochemistry, and dewetting, have been employed by researchers to alter or coat the surface of polymers with metal nanoparticles [10–13]. Recently, nanosized patterns with enhanced structural stability were produced on gold surfaces using reversible addition–fragmentation chain transfer (RAFT) PS [14]. Indeed, gold (Au) nanoparticles (NPs) are attracting a lot of interest due to their unexpected and high catalytic properties [3,15–17]. It was reported that Au NPs' size, shape, and support where the particles are attached/setting influence the catalytic activity of these NPs [18–20]. In some cases, the choice of support determines the type of Au NP application. For example, metal oxides, such as TiO_2, CeO_2, etc., are widely chosen as supports for Au NPs in catalytic oxidation and photo-catalysis applications [21–24]. Furthermore, carbon/polymer materials, with thiol [25,26] or amine functionalized surfaces [27,28], are another type of Au NP support for bio-sensing applications. In addition, Au NPS can also be attached to proteins (amino-acid structure with amine and carboxylic groups) for fighting cancer cells [29–31]. The anchoring of Au nanoparticles onto hydrophilic or hydrophobic polymer surfaces was investigated for the development of a virus-sensing platform [32]. Another study explored wettability and surface-enhanced Raman scattering in PMMA and PS free-standing films incorporated with embedded Au NP [33].

It is worth mentioning that the link between Au NPs and different chemical environments is crucial for improving the performance of these NPs for a given application. Although Au NPs are widely used in the applications mentioned above, the understanding of Au NPs' interaction with different functional groups has not been thoroughly investigated yet [31,34–36].

In this work, the interaction of Au NPs with amine, carboxylic, and fluorine functionalized surfaces was probed. The plasma surface modification of PS film, grafted with amine or carboxylic, or fluorine groups, was explored as a platform for Au NP deposition via the physical vapor deposition technique. XPS and atomic force microscope were employed as powerful surface characterization tools to probe the Au NP surface upon deposition on PS, both without and after plasma treatment. The results demonstrated evidence of Au interaction in different chemical environments. The findings add valuable information to the Au NPs/support interaction types owing to specific surface chemistries, which have implications in catalysis and sensing applications.

Initially, spin-coated PS film surfaces were modified using low-pressure plasma generated by electrical discharges in argon/ammonia (Ar/NH_3), argon/oxygen (Ar/O_2), or argon/tetrafluoroethane ($Ar/C_2H_2F_4$) gas mixtures. The plasma treatments were conducted under controlled conditions, thus preserving the PS surface, while incorporating various chemical groups for different gas mixtures. The surface of PS films, before and after the treatment, was characterized using X-ray photoelectron spectroscopy (XPS) and contact angle measurements. Then, Au NP was deposited over PS films with no plasma treatment or after treatment in specific plasma conditions. This was followed by extensive XPS analysis to investigate the Au NPs' interaction with PS before and after surface modification.

2. Experimental Details

2.1. Spin Coating of Polystyrene Films

The polymer used in this study was polystyrene (PS) (MW 280,000) received from Borealis Stenung sund, Sweden. As a solvent for PS, anhydrous toluene (99.8% purity, Sigma Aldrich) was arranged. For complete dissolution, the PS solution in toluene was heated at 50 °C for 2 h. From solution with 3% dissolved PS, films were spin-coated onto silicon (100) coupons, with nominal dimensions of 20×20 mm^2, at 3000 rpm speed. As determined using a profilometer, PS films with thickness values in the 150–200 nm range were produced.

2.2. Plasma Treatment

The low-pressure plasma setup used for Au NP deposition over the PS films is schematically illustrated in Figure 1. The discharge was generated between two plane electrodes with the substrate placed on ground electrode (lower electrode) at a distance of 4 cm from the RF electrode. The discharge was ignited in gas mixtures containing argon and molecular oxygen, ammonia, or tetrafluoromethane at 10 and 25 sccm flow rates, respectively. The RF plasma power was maintained at 20 W, and the deposition process was carried out for 5 min. The experimental conditions have been listed in Table 1.
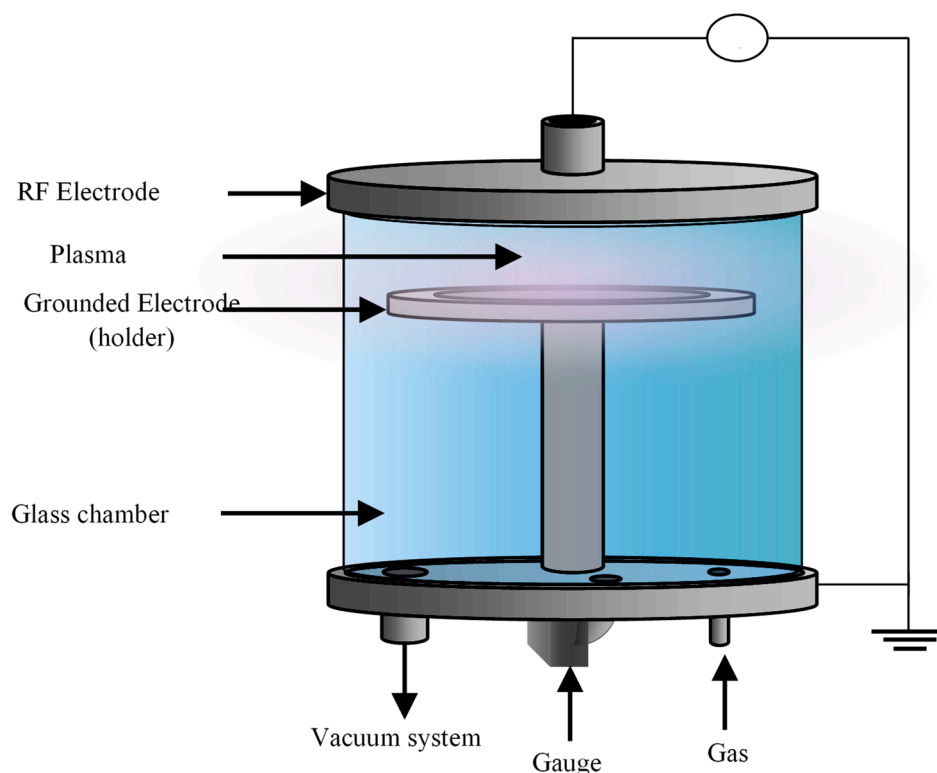
Figure 1. Schematic illustration of the low-pressure plasma treatment setup used for as-deposited PS films.

Table 1. Experimental conditions for plasma treatment of polymeric substrates and subsequent DC sputtering of gold nanoparticles.

Sample ID	Plasma Treatment: 20 W, 5 min		Gold Nanoparticles
	Pressure [mbar]	Reactive Species in Gas Mixture Ar:X 10:25 [sccm]	
As made	-	-	
Ar/O_2	0.35	O_2	9 W, 10 s, 30 sccm Ar flux, 5×10^{-3} mbar
Ar/NH_3	0.90	NH_3	
$Ar/C_2H_2F_4$	0.35	$C_2H_2F_4$	

2.3. Au NPs Deposition

Gold nanoparticles (Au NPs) were deposited onto PS films before and after plasma treatment via DC sputtering. The Au target (99.999% in purity, 2 in. diameter) was sputtered using Argon flux of 10 sccm at 9 W power and 5×10^{-3} mbar working pressure for 10 s each time. The equivalent thickness as measured by the quartz crystal micro-balance was ~1 nm each time and for all samples. Such thickness allows for the formation of well-dispersed

Au NPs. Table 1 depicts the experimental conditions for plasma treatment of PS surfaces and subsequent DC sputtering of Au NPs.

2.4. Materials Characterization

For surface chemistry analysis, XPS measurements were carried out using K-Alpha, (Thermo Scientific, East Grinstead, UK) with monochromatic (Al Kα) X-ray beam. The beam spot area was 300×300 μm, and the spectrometer was equipped with a flood gun for charge compensation. As a reference, the C 1s line of 284.5 eV was used to correct the binding energies for any charge energy shift. Shirley background was subtracted from the spectra and the signals, whereas symmetric Gaussian functions were used during the peak-fitting procedure on Casa XPS software version 2.3.25. The thicknesses of the films were estimated using a DEKTAK VEECO 8 profilometer. Condensation experiments and contact angle measurements were made to determine wettability. The contact angle measurements were performed using a KSV CAM101 instrument consisting of a single compact unit equipped with a FireWire video camera of 640×480 pixels resolution, a test stand, a standard syringe, and an LED source. The contact angle was measured using a wetting liquid. The experiments were performed at room temperature by placing a drop of 50 μL liquid (corresponding to a spherical drop of 500 μm radius) on the surface.

The surface morphology of the samples was characterized using atomic force microscope (AFM) operating in the contact mode (NanoWizard II BioAFM).

3. Results and Discussion

The fabrication process for the Au NPs/functionalized PS is shown schematically in Figure 2. It is noteworthy that the spin-coating method was used to deposit PS with an average thickness of 200 nm, which serves as the base polymer in the proposed fabrication process. First, the silicon substrate is immersed in acetone and then isopropanol for ultrasonic vibrations for 5 and 2 min, respectively. The main objective of this cleaning step is to avoid any contribution of surface contamination to the surface functionalities. The clean surface is essential for the next step when the PS suspension is spinning and cast onto the substrate to achieve a uniform film. During the next step, the PS film surface is treated with different plasma types to introduce a desirable functional group over the surface. This is accomplished by exposing the PS support film to an RF plasma with the parameters listed in Table 1. As the final step, a conformal gold layer with a thickness of about 1 nm is deposited on the functionalized PS film.
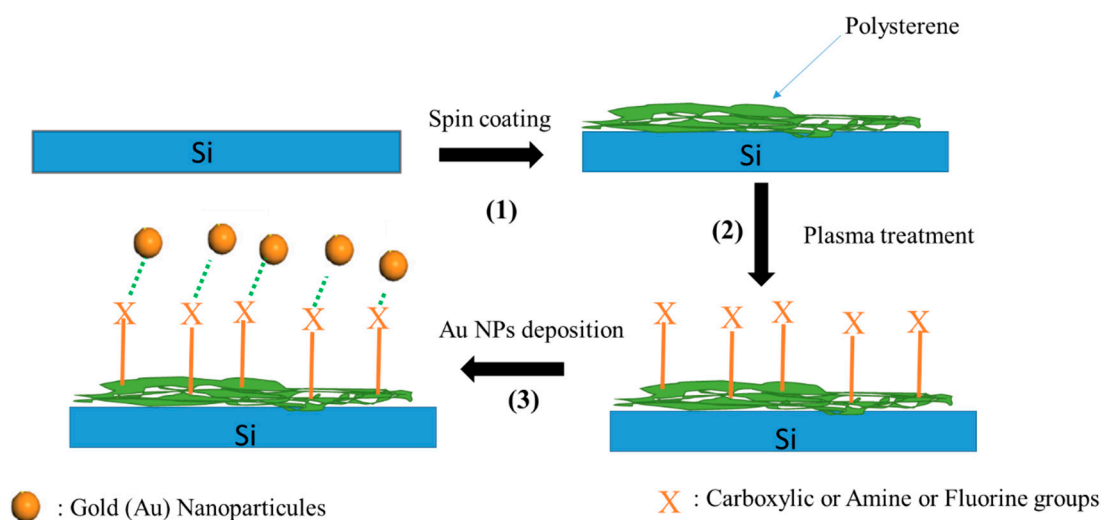

Figure 2. Schematic view of spin-coated PS deposition on Si substrates (**1**) followed by plasma treatment (**2**) and gold NP deposition (**3**).

The SEM image of the PS film (Figure 3) shows a smooth surface, which will be further examined under AFM in the following section. The film thickness, as estimated from the diamond stylus-based contact profilometer, was ~180 nm. The PS film was chosen as a virgin platform for the attachment of different chemical groups since it contains only carbon and hydrogen and is easy to be functionalized at low temperatures. Due to the very low thin and smooth film, surface morphology could not be revealed. The area shown in Figure 3 represents a small polymeric segment protruding out of the otherwise very smooth film. The edge of the flake-like feature also confirms the film thickness to be sub-micron.
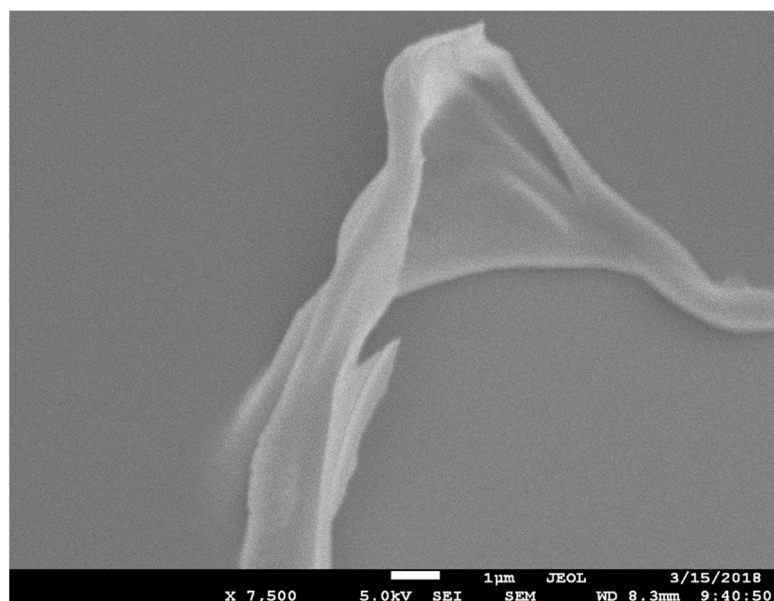

Figure 3. Top view SEM image of PS film deposited on Si substrate.

XPS survey spectra of the untreated and plasma-modified PS films are presented in Figure 4. The carbon element is omnipresent for all samples at 285 eV binding energy (the binding energy is charge corrected in all the XPS spectra). The untreated PS film exhibits the presence of 99.6% carbon at the surface, implying it is contamination-free since it only consists of aromatic and aliphatic carbon as well as hydrogen (not detectable by XPS). After plasma treatment, a strong nitrogen peak at 401 eV is detected that accounts for 0.8, 7.5, and 2.2 at.% nitrogen of the surface atomic composition after $Ar/C_2H_4F_4$, Ar/NH_3, and Ar/O_2 plasma treatments, respectively. The area of oxygen peak at 531 eV is noticed to increase from 0.4% for pristine PS surface to 4.5, 35.4, and 45.6 at%, respectively, upon modification with $Ar/C_2H_4F_4$, Ar/NH_3, and Ar/O_2 plasma. After $Ar/C_2H_4F_2$ plasma treatment, a strong intense new peak is observed at 688.0 eV that may be associated with F 1s with 69.7 at% of all the elements. The relatively low nitrogen content suggests the presence of nitrogen atoms only on the extreme upper level of the modified PS surface with presumably a few nanometers depth. This is due to the fact that the depth of analysis in the case of the XPS technique is limited to ~10 nm, considering the photoelectron take-off angle in the spectrometer to be 90°. It may be surprising that the relative amount of oxygen is also more important than that of nitrogen after Ar/NH_3 plasma treatment. However, plasma treatment activates the surface via the generation of free radicals and other charged species. These species can react with the surface and/or with other molecules present in the atmosphere of the plasma chamber, and later with ambient air once the substrate is exposed to the atmosphere during post-plasma treatment storage. The surface chemistry evolution will depend on the environment to which the surface is exposed to after plasma treatment [34]. In that case, post-treatment exposure to air or water, for instance, may yield significantly different surface chemistries for the same plasma-modified surface [37]. The

film surface chemistry and composition, as estimated by XPS, before and after plasma treatment, are graphically presented in Figure 4b.
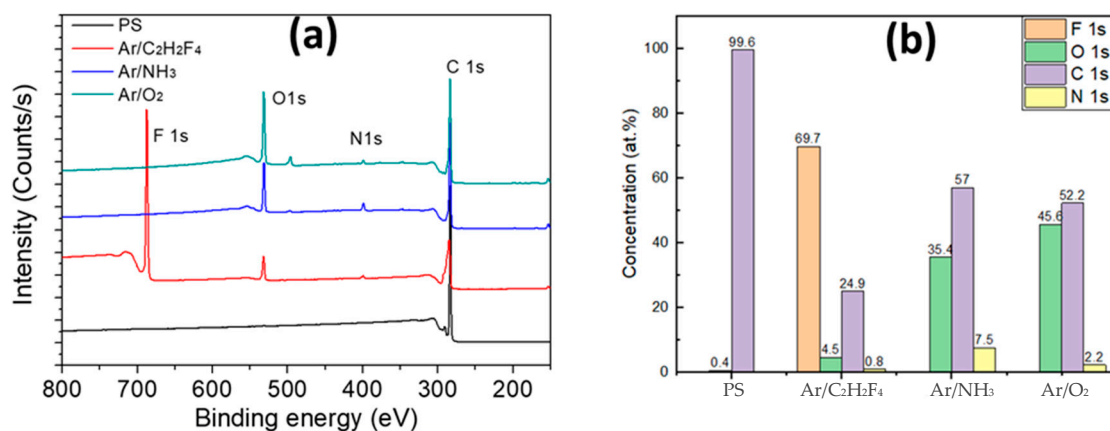

Figure 4. (**a**) XPS Survey spectra (**b**) elemental composition of as-deposited PS and PS after plasma treatment.

A comparison of the carbon peaks before and after plasma treatment is made, as shown in Figure 5. Untreated PS only exhibits one large peak caused by the C-C aliphatic chains and -C=C bonds from the phenyl ring [38]. Another minor peak, a satellite π-π* peak that is common in aromatic polymers, can be seen at a high binding energy of ~291.0 eV [39]. The carbon peak in the plasma-treated samples shows a noticeable change in shape, indicating the development of several functional groups at the surface. It is possible to identify functional groupings by breaking down the observed peak into two or more constituent component peaks, as indicated in Figure 5. When NH_3 is added to argon plasma, NH_x-based species are produced that interact with the PS surface [40,41]. The component in the C1s signal at the binding energy (BE) of 284.6 eV was much decreased in intensity by ammonia addition; however, the components at about BE $\approx$ 286 eV and BE $\approx$ 288 eV was strongly increased. The peak positions as well as the intensities of the subpeaks are too high to be interpreted as NH and NH_2 groups. The peak positioned at 287 eV may be more likely to be assigned as carbonyl functional groups (C=O and O-C-O) formed during the post-plasma phase. Figure 5c demonstrates how the inclusion of fluorine leads to the attachment of various functional groups, including CF_3, CF_2, and C-HF [8,42]. Figure 5d revealed a set of four distinct peaks appearing because of the Ar/O_2 treatment process. The maximum of each peak was shifted toward higher energies with respect to the hydrocarbon signal at 284.6 eV, which is consistent with the formation of oxidized units in the polymer chains [43]. The peak at 286 eV reveals the presence of carbonyl groups (C=O) at the surface yet may equally relate to carbon associated with two oxygen atoms (e.g., O-C-O). The peak at 289 eV corresponds to carbon in acid and ester groups (O-C=O). Finally, the spectrum showed a shakeup energy peak at 291.8 eV, accounting for the π-π* bond, which is assigned to the undamaged benzene ring in the PS surface [43].

To assess the effect of plasma treatment on the wetting characteristics of PS films, water contact angle (WCA) measurements were performed on all the samples. The WCA values for untreated and plasma-modified PS films are showcased in Figure 6. The WCA values were noticed to decrease from 98° for the untreated PS, to 95°, 37°, and 17°, respectively, for the PS film surfaces treated with $Ar/C_2H_2F_4$, Ar/NH_3, and Ar/O_2 plasma. This reduction in the contact angle values reveals a progressive transformation in the PS surface wettability from strongly hydrophobic to weak hydrophobic or even hydrophilic. It is a well-known fact that the water-repellent tendency of a solid surface depends on two factors: (i) the surface chemistry and functionality and (ii) the surface micro/nano morphological features. Since the surface morphology was practically not affected in our experiments, the modification of contact angles due to plasma treatment may be attributed to the incorporation of nitrogen/oxygen-based groups into the film surfaces, as already confirmed

from XPS analysis. The PS-treated film surface produced many free radicals, such as -OH, -COOH, and -C=O, which increased the polarity of the films, increasing their hydrophilicity and lowering the water contact angle value. Matouk et al. already demonstrated that a DBD treatment of cellulose nanocrystals surface with Ar /NH$_3$ plasma produced polar functional groups, such as C-O/C-N, C=O/O=C-N, that in turn, cause an increase in the film hydrophilicity [43].
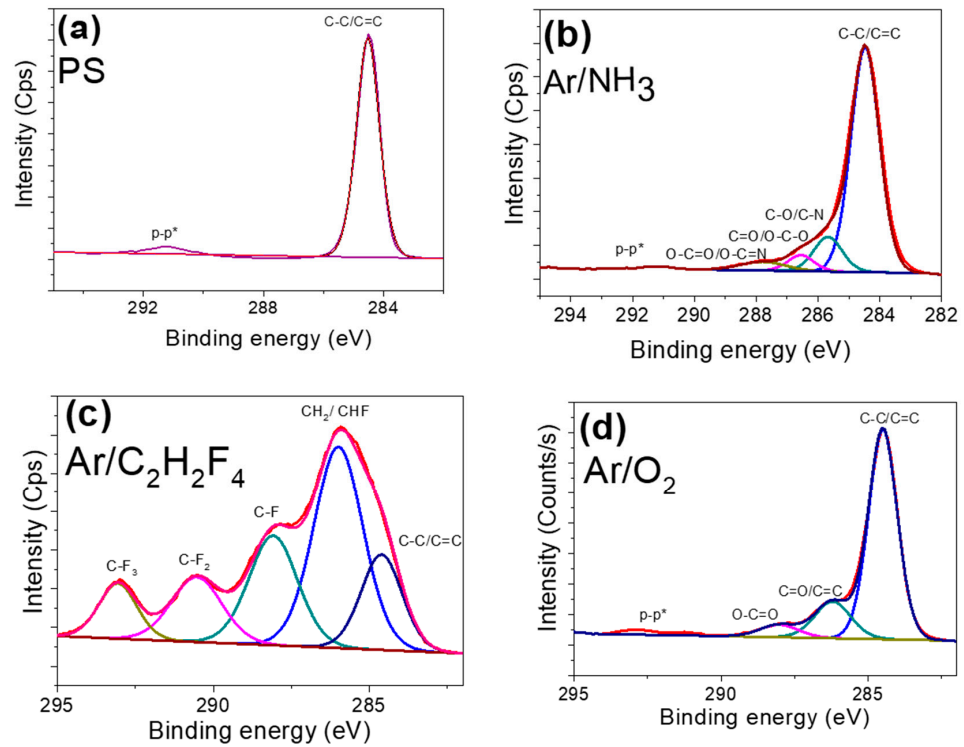
Figure 5. High-resolution spectrum of the C 1s signal of (**a**) pristine PS, (**b**) Ar/NH$_3$, (**c**) Ar/C$_2$H$_2$F$_4$, and (**d**) Ar/O$_2$ plasma-treated samples.
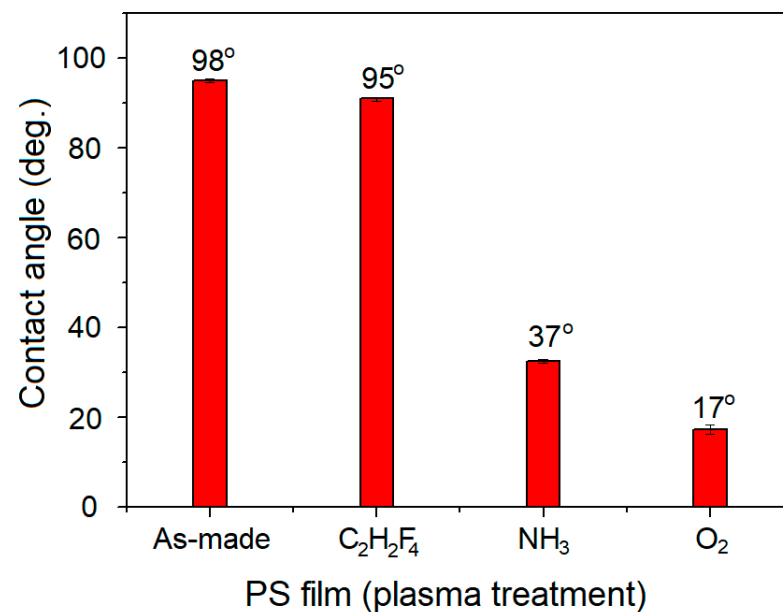
Figure 6. Water contact angle values for the as-deposited (untreated) and functionalized PS films after plasma treatment in argon (Ar) gas admixed with tetrafluoromethane (C$_2$H$_2$F$_4$), ammonia (NH$_3$), and oxygen (O$_2$).

The TEM micrographs of Au NPs deposited onto the PS are shown in Figure 7a,b. In some regions (Figure 7a), one can observe the agglomeration of Au NPs with different size distributions. The microstructure recorded at the substrate edge (Figure 7b) demonstrates the presence of isolated Au NPs, thus indicating an inhomogeneous type of Au NP deposition at the PS support surface.
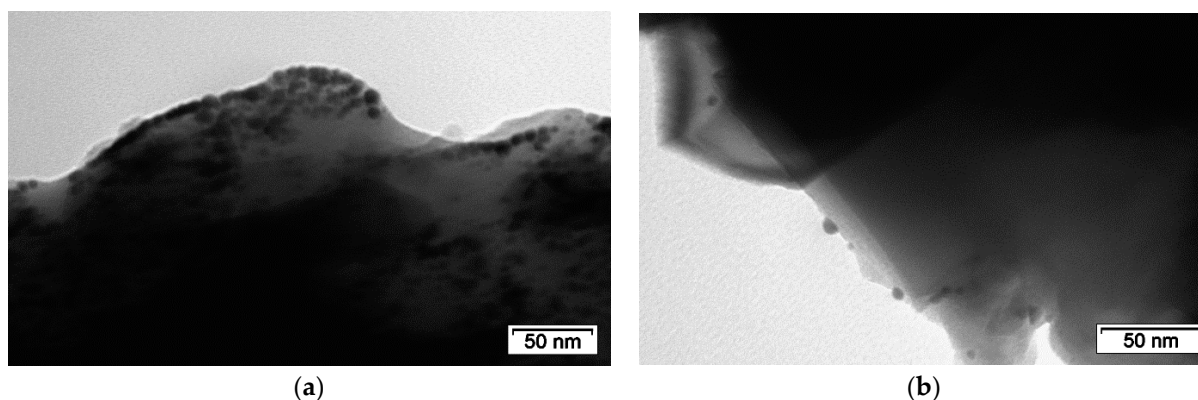

(**a**)   (**b**)

Figure 7. (**a**) Au NP clusters formed on the as-deposited PS surface and (**b**) few isolated Au NPs.

The Au NP-supported PS film surfaces with distinct chemistries were thoroughly investigated as support surfaces to determine the nature of their mutual interactions. Even though Au is classified as a poor catalyst because of its chemical inertness towards the chemisorption of reactive molecules, its nanoparticles are extremely active because of the creation of metal/oxide interfaces. The localized surface plasmon resonance (LSPR) effect, which causes electron injection from the Au NP to PS conduction band for subsequent reduction of the adsorbed molecular oxygen, is one potential mechanism for photocatalytic activity enhancement during organic molecule photodegradation. Through oxidation of the organic molecule, the electron-deficient Au is gradually restored to its metallic condition [44].

Figure 8 shows the XPS Au 4f core level spectra for the Au NPs deposited on either untreated or plasma-modified PS films. For the untreated PS film, the Au 4f peak, located at 84.1 eV, represents Au in the metallic state [43,45]. This implies that every sample of the Au NPs is in a charge-neutral, bulk-like state. There was no shift in the XPS Au 4f peak position arising from Au NPs deposition on the $Ar/C_2H_2F_4$ plasma modified PS surface, thus suggesting that there is no evidence of any chemical interaction between the Au NPs and the PS support polymer with fluorine groups. However, a negative binding energy shift of about 0.2 eV for the Au 4f peak was noticed in the case of Au NPs deposited on Ar/NH_3 plasma functionalized PS film. On the other hand, a positive binding energy shift of about 0.2 eV for the Au 4f peak was also measured in the case of Au NPs deposited over Ar/O_2 plasma-treated PS.

In principle, such a shift toward low binding energies for an Au metal may be related either to (i) an electron screening effect due to variations in Au cluster size with film thickness variation or (ii) an electron donation from the PS films with amine groups to the Au. Since the size of Au NPs deposited on PS film before and after Ar/NH_3 plasma treatment is the same, the effect of electron screening can be ruled out. Therefore, this shift toward low binding energy is evidence of strong interaction between Au NPs and the amine groups present in the Ar/NH_3 plasma-treated PS films. Indeed, an electron donation from amine groups toward Au NPs has already been reported [26,46]. For the high energy shift (about 0.2 eV) of the Au 4f band compared to Au NPs attached to PS, one can assume an electron donation from the Au NPs cluster to the oxygen/carbon group. Such a shift toward high binding energies has already been observed in the case of Au NPs deposited on oxygen plasma-treated carbon nanotubes [47].

Figure 9 presents AFM area scans for the different Au/PS film surfaces. The 200 nm × 200 nm scan areas reveal that the coatings comprised fine-grained, nanosized, and homogeneously distributed Au NPs. In general, the particles do not form larger clusters within layers nor tend to align into higher-order patterns. Such a result suggests immobilized adsorption of sputtered blocks of the target material with no subsequent surface diffusion due likely to the low substrate temperature. It is deduced that the deposition cycle devised for this work produces smooth films having a granular structure with root-mean-square (RMS) value typically below 1 nm and highly isotropic spatial characteristics with anisotropy ratio (S_{tr}) being above 0.83. It is noteworthy that surface roughness is highly correlated with the concentration of the particles, and a high number of particles per unit area results in smoother deposits due to enhanced filling of surface voids.
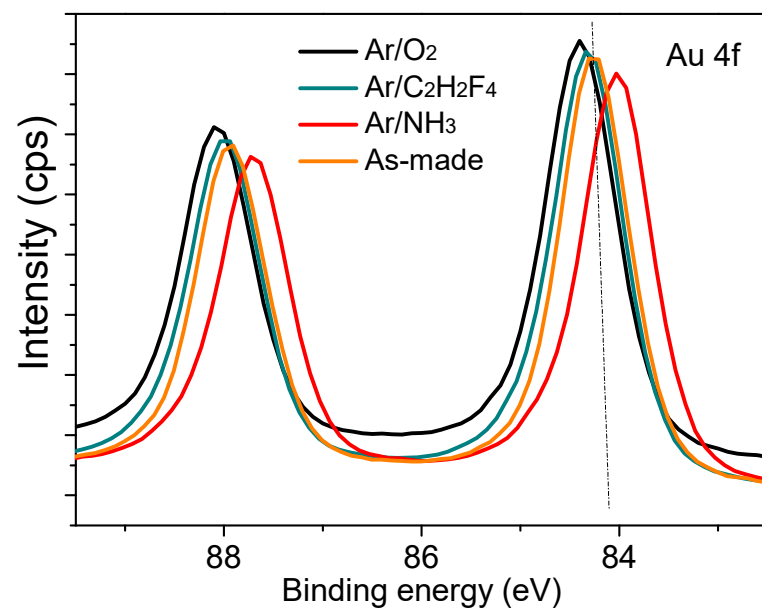

Figure 8. XPS Au 4f core level spectra of deposited on as made PS and plasma treated PS within argon (Ar) gas admixed with tetrafluoromethane ($C_2H_2F_4$), ammonia (NH_3), and oxygen (O_2).

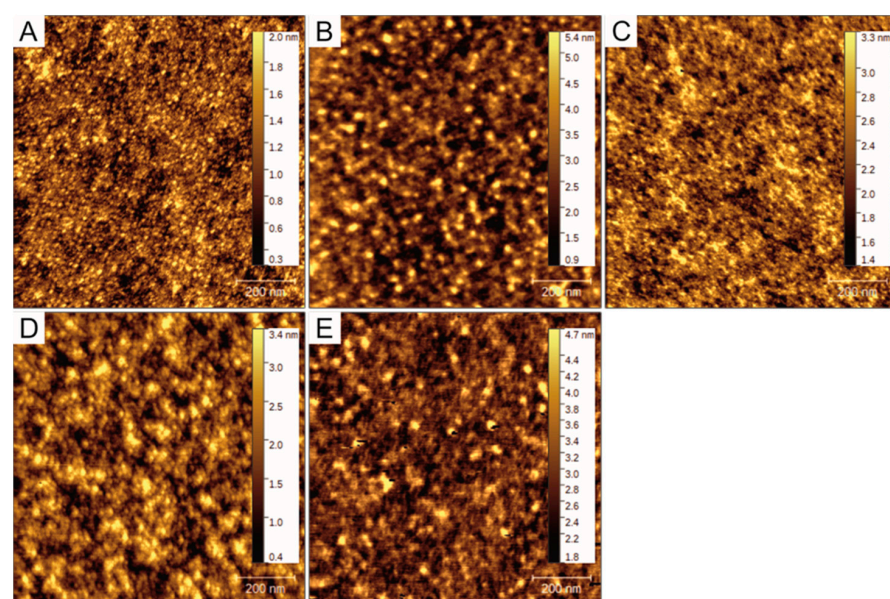**Figure 9.** AFM images of Au NPs sputtered on a PS-coated silicon wafer (200 × 200 nm^2 scan area): (**A**) PS film, (**B**) Untreated Au NPs/PS, (**C**) Ar/NH_3 plasma-treated Au NPs/PS film, (**D**) Ar/O_2 plasma-treated Au NPs/PS film, and (**E**) Ar/$C_2H_2F_4$ plasma-treated Au NPs/PS film.

The reference sample (untreated PS film), shown in Figure 9A, is found to be the smoothest among all the films prepared, revealing homogeneity in surface patterns. Figure 9B reveals that DC sputtering alone (no plasma treatment of the PS film) yields the flattest structure with nanoparticles having 5–15 nm diameter. Small Au islands are well dispersed and cover the surface forming a homogeneous, isotropic structure. Ar/NH_3 plasma treated PS film (Figure 9C) also constitutes of fine-grained structure with area density and average size for the Au NPs of 960 μm^{-2} and ~10 nm, respectively, and a surface coverage of ~5% of the examined area. According to previous observations, high particle concentration implies low surface roughness (0.331 nm). Ar/O_2 plasma treated PS film supporting Au NPs (Figure 9D) is found to exhibit a coarse grain structure with a low particle area density of ~380 μm^{-2}, although the average nanoparticle size (19–26 nm), relative surface coverage (9.7%), and surface roughness (0.632 nm) were significantly greater. The surface morphology of the Au NPs/PS film ($Ar/C_2H_2F_4$ plasma modified), as shown in Figure 9E, appears similar in morphology to that presented in Figure 9D, with similar anisotropy ratio (0.92–0.94) and mean NPs size of the order of ~20 nm.

4. Conclusions

Spin-coated polystyrene (PS) films, when subjected to plasma treatment in different gas mixtures, have different functional groups incorporated onto their surface depending on the plasma gas mixture, without any disruption to the surface morphology. Plasma treatment leads to improvement in film hydrophilicity due to chemical modification of the PS film surface. Among oxygen (O_2), ammonia (NH_3), and tetrafluoroethane ($C_2H_2F_4$) added to argon (Ar), the Ar/O_2 plasma treatment is more efficient towards rendering PS hydrophilic, while plasma treatments with Ar/NH_3 and $Ar/C_2H_2F_4$ gas mixture show almost similar results for any improvement in film hydrophilicity. Such change may be primarily attributed to the oxygen groups and surface roughness present on the surface of films treated in the Ar/O_2 plasma, as supported by XPS and AFM analyses. XPS analysis showed that Au NPs' sputter deposition onto plasma-modified PS films induced a chemical shift in the metallic Au NPs peak positioned at 84.1 eV. This is direct evidence of interaction between Au NPs and different chemical groups attached to the PS surface. Moreover, it was found that Ar/NH_3 plasma led to a low binding energy shift, whereas Ar/O_2 plasma treatment resulted in a high binding energy shift. Such a shift may be attributed to electron donation and acceptance from Au NPs in case of high and low binding energy shifts, respectively. Au/PS films with tailored surface energy and degree of hydrophilicity have strong potential for use in catalysis and sensing applications involving certain nanopatterns.

Author Contributions: Conceptualization, A.A. and M.I.; Methodology, N.O., A.A. and Z.M.; Validation, M.I. and J.-J.P.; Formal analysis, N.O., M.I., Z.M. and A.A.; Investigation, Z.M.; Resources, J.-J.P.; Data curation, N.O. and Z.M.; Writing—original draft, M.I. and A.A.; Writing—review and editing, A.A. and M.I.; Visualization, M.I.; Supervision, A.A.; Project administration, J.-J.P. All authors have read and agreed to the published version of the manuscript.

Data Availability Statement: Data is contained within the article.

References

1. Gurman, J.L.; Baier, L.; Levin, B.C. Polystyrenes: A Review of the Literature on the Products of Thermal Decomposition and Toxicity. NIST Interagency/Internal Rep. 1986. Available online: https://www.nist.gov/publications/polystyrenes-review-literature-products-thermal-decomposition-and-toxicity (accessed on 29 November 2022).
2. Cooper, I. Plastics and chemical migration into food. *Chem. Migr. Food Contact Mater.* **2007**, *1*, 228–250. [CrossRef]
3. Wünsch, J.R. *Polystyrene: Synthesis, Production and Applications*; Rapra Technology Ltd.: Shawbury, UK, 2000; Volume 10.
4. Haider, S.; Kausar, A.; Muhammad, B. Overview on Polystyrene/Nanoclay Composite: Physical Properties and Application. *Polym. Technol. Eng.* **2017**, *56*, 917–931. [CrossRef]

5. Cai, S.; Zhang, B.; Cremaschi, L. Review of moisture behavior and thermal performance of polystyrene insulation in building applications. *Build. Environ.* **2017**, *123*, 50–65. [CrossRef]

6. Liston, E.M.; Martinu, L.; Wertheimer, M.R. Plasma surface modification of polymers for improved adhesion: A critical review. *J. Adhes. Sci. Technol.* **1993**, *7*, 1091–1127. [CrossRef]

7. Yasuda, H. Plasma treatment for improved bonding: A review. *J. Macromol. Sci. Part A Chem.* **1976**, *30*, 199–218.

8. Matouk, Z.; Torriss, B.; Rincón, R.; Dorris, A.; Beck, S.; Berry, R.M.; Chaker, M. Functionalization of cellulose nanocrystal films using Non-Thermal atmospheric–Pressure plasmas. *Appl. Surf. Sci.* **2020**, *511*, 145566. [CrossRef]

9. Beaulieu, I.; Geissler, M.; Mauzeroll, J. Oxygen Plasma Treatment of Polystyrene and Zeonor: Substrates for Adhesion of Patterned Cells. *Langmuir* **2009**, *25*, 7169–7176. [CrossRef]

10. Tian, X.; Yu, Q.; Kong, X.; Zhang, M. Preparation of Plasmonic Ag@PS Composite via Seed-Mediated In Situ Growth Method and Application in SERS. *Front. Chem.* **2022**, *10*, 142. [CrossRef]

11. Calis, B.; Yilmaz, M. Fabrication of gold nanostructure decorated polystyrene hybrid nanosystems via poly(L-DOPA) and their applications in surface-enhanced Raman Spectroscopy (SERS), and catalytic activity. *Colloids Surfaces A Physicochem. Eng. Asp.* **2021**, *622*, 126654. [CrossRef]

12. Eisen, C.; Ge, L.; Santini, E.; Gia, M.C.; Reithofer, M.R. Hyper crosslinked polymer supported NHC stabilized gold nanoparticles with excellent catalytic performance in flow processes. *Nanoscale Adv.* **2023**, *5*, 1095–1101. [CrossRef]

13. Li, H.; Li, A.; Zhao, Z.; Li, M.; Song, Y. Heterogeneous Wettability Surfaces: Principle, Construction, and Applications. *Small Struct.* **2020**, *1*, 2000028. [CrossRef]

14. Hendrich, K.; Peng, W.; Vana, P. Controlled Arrangement of Gold Nanoparticles on Planar Surfaces via Constrained Dewetting of Surface-Grafted RAFT Polymer. *Polymers* **2020**, *12*, 1214. [CrossRef]

15. Das, M.; Shim, K.H.; An, S.S.A.; Yi, D.K. Review on gold nanoparticles and their applications. *Toxicol. Environ. Health Sci.* **2012**, *3*, 193–205. [CrossRef]

16. Al-Hamdani, A.H.; A Madlool, R.; Abdulazeez, N.Z. Effect of gold nanoparticle size on the linear and nonlinear optical properties. *AIP Conf. Proc.* **2020**, *2290*, 050029.

17. Trudel, S. Unexpected magnetism in gold nanostructures: Making gold even more attractive. *Gold Bull.* **2011**, *44*, 3–13. [CrossRef]

18. Zhuang, Y.; Liu, L.; Wu, X.; Tian, Y.; Zhou, X.; Xu, S.; Xie, Z.; Ma, Y. Size and Shape Effect of Gold Nanoparticles in "Far-Field" Surface Plasmon Resonance. *Part. Part. Syst. Charact.* **2019**, *36*, 1800077. [CrossRef]

19. Lin, C.; Tao, K.; Hua, D.; Ma, Z.; Zhou, S. Size Effect of Gold Nanoparticles in Catalytic Reduction of p-Nitrophenol with NaBH4. *Molecules* **2013**, *18*, 12609–12620. [CrossRef]

20. Sankar, M.; He, Q.; Engel, R.V.; Sainna, M.A.; Logsdail, A.J.; Roldan, A.; Willock, D.J.; Agarwal, N.; Kiely, C.J.; Hutchings, G.J. Role of the Support in Gold-Containing Nanoparticles as Heterogeneous Catalysts. *Chem. Rev.* **2020**, *120*, 3890–3938. [CrossRef]

21. Solaymani, S.; Yadav, R.P.; Ţălu, Ş.; Achour, A.; Rezaee, S.; Nezafat, N.B. Averaged power spectrum density, fractal and multifractal spectra of Au nano-particles deposited onto annealed TiO$_2$ thin films. *Opt. Quantum Electron.* **2020**, *52*, 1–16. [CrossRef]

22. García, T.; López, J.M.; Solsona, B.; Sanchis, R.; Willock, D.J.; Davies, T.E.; Lu, L.; He, Q.; Kiely, C.J.; Taylor, S.H. The Key Role of Nanocasting in Gold-based Fe$_2$O$_3$ Nanocasted Catalysts for Oxygen Activation at the Metal-support Interface. *Chemcatchem* **2019**, *11*, 1915–1927. [CrossRef]

23. Li, L.; Liu, Y.; Wang, Q.; Zhou, X.; Li, J.; Song, S.; Zhang, H. CeO$_2$ supported low-loading Au as an enhanced catalyst for low temperature oxidation of carbon monoxide. *Crystengcomm* **2019**, *21*, 7108–7113. [CrossRef]

24. Achour, A.; Islam, M.; Solaymani, S.; Vizireanu, S.; Saeed, K.; Dinescu, G. Influence of plasma functionalization treatment and gold nanoparticles on surface chemistry and wettability of reactive-sputtered TiO2 thin films. *Appl. Surf. Sci.* **2018**, *458*, 678–685. [CrossRef]

25. Xue, Y.; Li, X.; Li, H.; Zhang, W. Quantifying thiol–gold interactions towards the efficient strength control. *Nat. Commun.* **2014**, *5*, 4348. [CrossRef] [PubMed]

26. Achour, A.; Solaymani, S.; Vizireanu, S.; Baraket, A.; Vesel, A.; Zine, N.; Errachid, A.; Dinescu, G.; Pireaux, J. Effect of nitrogen configuration on carbon nanowall surface: Towards the improvement of electrochemical transduction properties and the stabilization of gold nanoparticles. *Mater. Chem. Phys.* **2019**, *228*, 110–117. [CrossRef]

27. Lee, G.; Lee, H.; Nam, K.; Han, J.-H.; Yang, J.; Lee, S.W.; Yoon, D.S.; Eom, K.; Kwon, T. Nanomechanical characterization of chemical interaction between gold nanoparticles and chemical functional groups. *Nanoscale Res. Lett.* **2012**, *7*, 608. [CrossRef]

28. Ponraj, S.B.; Chen, Z.; Li, L.H.; Shankaranarayanan, J.S.; Rajmohan, G.D.; du Plessis, J.; Sinclair, A.J.; Chen, Y.; Wang, X.; Kanwar, J.R.; et al. Fabrication of Boron Nitride Nanotube–Gold Nanoparticle Hybrids Using Pulsed Plasma in Liquid. *Langmuir* **2014**, *30*, 10712–10720. [CrossRef]

29. Bai, X.; Wang, Y.; Song, Z.; Feng, Y.; Chen, Y.; Zhang, D.; Lin, F. The Basic Properties of Gold Nanoparticles and their Applications in Tumor Diagnosis and Treatment. *Int. J. Mol. Sci.* **2020**, *21*, 2480. [CrossRef]

30. Balfourier, A.; Luciani, N.; Wang, G.; Lelong, G.; Ersen, O.; Khelfa, A.; Alloyeau, D.; Gazeau, F.; Carn, F. Unexpected intracellular biodegradation and recrystallization of gold nanoparticles. *Proc. Natl. Acad. Sci. USA* **2020**, *117*, 103–113. [CrossRef]

31. Sändig, N.; Zerbetto, F. Molecules on gold. *Chem. Commun.* **2010**, *46*, 667–676. [CrossRef]

32. Carnerero, J.M.; Jimenez-Ruiz, A.; Castillo, P.M.; Prado-Gotor, R. Covalent and non-covalent DNA-gold-nanoparticle interactions: New avenues of research. *Chemphyschem* **2017**, *18*, 17–33. [CrossRef]

33. Ahmed, S.R.; Kim, J.; Tran, V.T.; Suzuki, T.; Neethirajan, S.; Lee, J.; Park, E.Y. In situ self-assembly of gold nanoparticles on hydrophilic and hydrophobic substrates for influenza virus-sensing platform. *Sci. Rep.* **2017**, *7*, srep44495. [CrossRef]

34. Prasad, M.D.; Krishna, M. Au nanoparticle embedded Poly(methyl-methacrylate) and Poly(styrene) free-standing films for wettability and surface enhanced Raman scattering applications. *Mater. Sci. Eng. B* **2021**, *272*, 115324. [CrossRef]

35. Arshad, M.; Karamti, H.; Awrejcewicz, J.; Grzelczyk, D.; Galal, A.M. Thermal Transmission Comparison of Nanofluids over Stretching Surface under the Influence of Magnetic Field. *Micromachines* **2022**, *13*, 1296. [CrossRef]

36. Arshad, M.; Hussain, A.; Elfasakhany, A.; Gouadria, S.; Awrejcewicz, J.; Pawłowski, W.; Elkotb, M.A.; Alharbi, F.M. Magneto-Hydrodynamic Flow above Exponentially Stretchable Surface with Chemical Reaction. *Symmetry* **2022**, *14*, 1688. [CrossRef]

37. Ghasemi, M.; Minier, M.; Tatoulian, M.; Arefi-Khonsari, F. Determination of Amine and Aldehyde Surface Densities: Application to the Study of Aged Plasma Treated Polyethylene Films. *Langmuir* **2007**, *23*, 11554–11561.

38. Biesinger, M.C. Accessing the robustness of adventitious carbon for charge referencing (correction) purposes in XPS analysis: Insights from a multi-user facility data review. *Appl. Surf. Sci.* **2022**, *597*, 153681. [CrossRef]

39. Morgan, D.J. Comments on the XPS Analysis of Carbon Materials. *C* **2021**, *7*, 51. [CrossRef]

40. López-Santos, C.; Yubero, F.; Cotrino, J.; Contreras, L.; Barranco, A.; González-Elipe, A.R. Formation of Nitrogen Functional Groups on Plasma Treated DLC. *Plasma Process. Polym.* **2009**, *6*, 555–565. [CrossRef]

41. Vesel, A.; Junkar, I.; Cvelbar, U.; Kovac, J.; Mozetic, M. Surface modification of polyester by oxygen- and nitrogen-plasma treatment. *Surf. Interface Anal.* **2008**, *40*, 1444–1453. [CrossRef]

42. Fluorovo, H.P. Hydrophobization of polymer polystyrene in fluorine plasma. *Mater. Tehnol.* 2011. Available online: http://mit.imt.si/izvodi/mit113/vesel.pdf (accessed on 29 November 2022).

43. Sakai, Y.; Norimatsu, H.; Saito, Y.; Inomata, H.; Mizuno, T. Silica coating on plastics by liquid phase deposition (LPD) method. *Thin Solid Films* **2001**, *392*, 294–298. [CrossRef]

44. Casaletto, M.P.; Longo, A.; Martorana, A.; Prestianni, A.; Venezia, A.M. XPS study of supported gold catalysts: The role of Au0 and Au+δ species as active sites. *Surf. Interface Anal.* **2006**, *38*, 215–218. [CrossRef]

45. Boccia, A.; Zanoni, R.; Arduini, A.; Pescatori, L.; Secchi, A. Structural electronic study via XPS and TEM of subnanometric gold particles protected by calixarenes for silicon surface anchoring. *Surf. Interface Anal.* **2012**, *44*, 1086–1090. [CrossRef]

46. Xie, X.; Long, J.; Xu, J.; Chen, L.; Wang, Y.; Zhang, Z.; Wang, X. Nitrogen-doped graphene stabilized gold nanoparticles for aerobic selective oxidation of benzylic alcohols. *RSC Adv.* **2012**, *2*, 12438–12446. [CrossRef]

47. Suarez-Martinez, I.; Bittencourt, C.; Ke, X.; Felten, A.; Pireaux, J.; Ghijsen, J.; Drube, W.; Van Tendeloo, G.; Ewels, C. Probing the interaction between gold nanoparticles and oxygen functionalized carbon nanotubes. *Carbon* **2009**, *47*, 1549–1554. [CrossRef]